JACS
JOURNAL OF THE AMERICAN CHEMICAL SOCIETY
Article
pubs.acs.org/JACS
Terms of Use

Precision Polymers and 3D DNA Nanostructures: Emergent Assemblies from New Parameter Space

Christopher J. Serpell, Thomas G. W. Edwardson, Pongphak Chidchob, Karina M. M. Carneiro, and Hanadi F. Sleiman*

Department of Chemistry and Centre for Self-assembled Chemical Structures, McGill University, 801 Sherbrooke Street West, Montreal, QC H3A 0B8, Canada

Supporting Information

ABSTRACT: Polymer self-assembly and DNA nanotechnology have both proved to be powerful nanoscale techniques. To date, most attempts to merge the fields have been limited to placing linear DNA segments within a polydisperse block copolymer. Here we show that, by using hydrophobic polymers of a precisely predetermined length conjugated to DNA strands, and addressable 3D DNA prisms, we are able to effect the formation of unprecedented monodisperse quantized superstructures. The structure and properties of larger micelles-of-prisms were probed in depth, revealing their ability to participate in controlled release of their constituent nanostructures, and template light-harvesting energy transfer cascades, mediated through both the addressability of DNA and the controlled aggregation of the polymers.

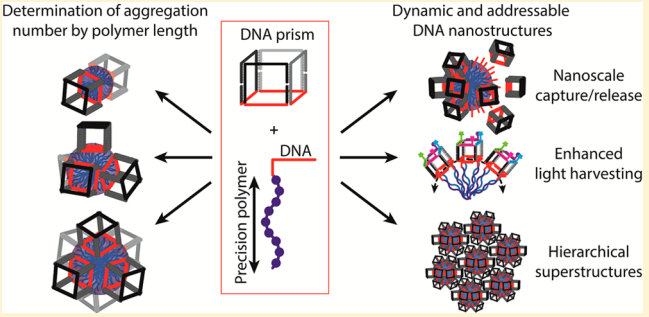

The progress of nanotechnology is driven by the discovery of new ways of organizing matter. One of the greatest leaps has been the introduction of DNA nanotechnology which permits the formation of anisotropic, molecularly monodisperse nanostructures through programmed recognition of nucleobase sequences.[1] Amphiphilic block copolymers that contain a water-soluble block, and a hydrophobic block also have the ability to self-assemble into a variety of predictable morphologies[2] and can be engineered for applications ranging from drug delivery to nanoelectronics and data storage. However, while the chemistry of block copolymers can be optimized for stability and biocompatibility, they lack the remarkable programmability, sequence selectivity, monodispersity, and fine structural control that DNA can offer. A particularly attractive goal is therefore the creation of block copolymers containing a 3D-DNA nanostructure as one of their blocks, uniting the programmability of DNA with the stability and ease of functionalization of synthetic polymers. On a fundamental level, this would give materials that derive their self-assembly properties not just from microphase separation of two blocks, but also from the highly ordered three-dimensional arrangement of the DNA block. We have observed that unusual self-assembled superstructures can be engineered when comparatively short hydrophobic groups are positioned correctly on DNA cubes.[3] Having recently developed a method for the synthesis of perfectly monodisperse and sequence-controlled polymers attached to DNA,[4] we now present an exploration of self-assembly in the new parameter-space thus revealed, that is, the position and number of polymer chains on the DNA cage, the geometry of the cage, and the exact number of repeat units on the polymer.

By accessing these variables, we can depart from the radially dominated structures typically generated by block copolymers. Instead, we approach the level of complexity demonstrated in proteins, where a large number of orthogonal noncovalent interactions operate in a cooperative manner to generate precise anisotropic architectures. Polymer–DNA conjugates have been reported previously,[5−8] and put to use in the construction of micelles[9] and vesicles,[10] and membrane models.[11] Typically, the self-assembly of these systems is undeveloped, resulting in radial arrangement of linear DNA strands around a hydrophobic polymer core. Examples of nonradial, anisotropic DNA as part of 3D DNA nanostructures in polymer systems are rare,[12,13] although small amphiphiles are beginning to emerge as tools to modulate, functionalize, and assemble DNA nanostructures.[14−17] To date, only one demonstration of polymer-mediated DNA superstructure formation has been reported, using a single polymer strand attached to a DNA tetrahedron;[13] however, the resultant structures required additional polymer assembly components, were of a range of sizes, and had not yet been enabled to partake in interactions with further nucleic acids or heterospecies, limiting further application. In contrast, we have now found that the confluence of precision polymers and 3D DNA nanostructures can lead to a collection of unique biohybrid structures. Variation of the position and multiplicity

Received: September 5, 2014
Published: October 17, 2014

   dx.doi.org/10.1021/ja509192n | J. Am. Chem. Soc. 2014, 136, 15767−15774

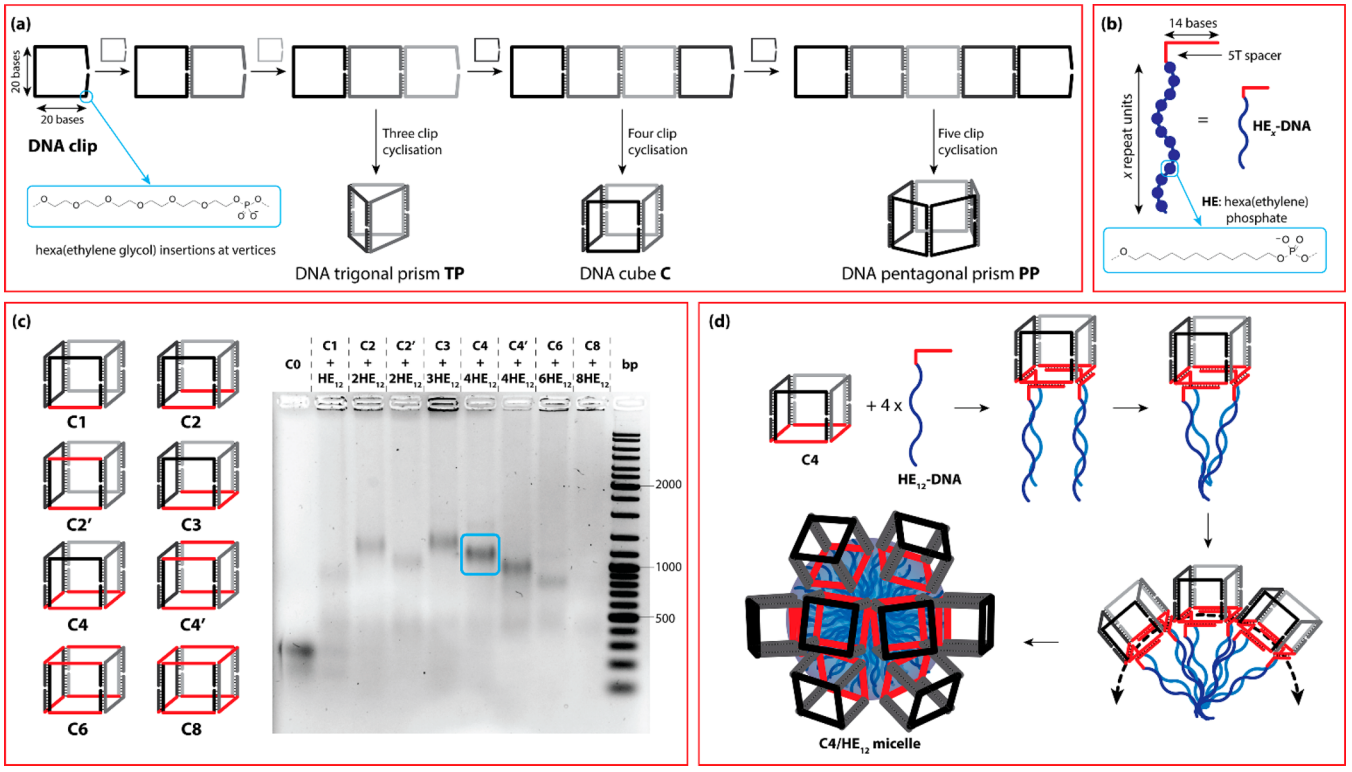

Figure 1. (a) Clip-by-clip assembly of prismatic DNA structures. (b) Structure of DNA–polymer conjugates HE_{12}-DNA. (c) Effect of variation of multiplicity and arrangement of HE_{12}-DNA on DNA cubes. Binding regions for HE_{12}-DNA are labeled in red. A compact band corresponding to a higher-order assembly is best seen in the C4 lane. The base-pair values in the marker lane, based upon linear duplexes, are not expected to correspond directly with 3D objects. (d) Formation of micelle-of-cubes by hydrophobic aggregation of HE_{12} chains attached to C4.

of the hydrophobic polymers on a DNA cage was used to find an optimal geometry for well-defined self-assembly. Altering the number of polymer repeat units on this cage led to quantization of DNA cage aggregation number; as the polymer length increases, monomeric (with polymer chains potentially aggregated on one face) structures gave way to dimer and discrete higher order assemblies with increasing finite aggregation number, after which monodisperse oligomeric micelles were seen. The versatility of the resultant superstructures was explored in the micelles, with the integrity of the DNA prisms on the surface being verified by their reversible binding and enzymatic assay. Variation of DNA prism size and geometry gave micelles of the same size, meaning that the number of prisms per micelle can be controlled in this manner. Addressability was demonstrated in the hybridization of DNA strands to their exterior resulting in predictable enlargement of the micelle, cross-linked aggregates, and the templation of light-harvesting cascades in which energy transfer is modified through micellization.

We anticipate that the library of unique nanostructures produced will provide new avenues for exploration in nanoscience, permitting new levels of controlled organization for electronically, optically, mechanically, or medicinally active nanostructures, and thus facilitate a fuller exploitation of the unique physical, chemical, and biological properties of the nanoscale.

RESULTS AND DISCUSSION

Prismatic scaffolds for the arrangement of polymers were constructed using the DNA-minimal "clip-by-clip" approach (Figure 1a).[18,19] The termini of each DNA clip strand were designed to hybridize with the central portion of a different clip forming a pseudomacrocycle which constitutes one face of the resultant prism. Further cyclization events yielded prisms, with a trigonal system requiring three clips, a cube four, and a pentagonal prism five. The intermediate regions on the clips remained available for hybridization with other strands. A library of clips was synthesized (Table S1, Figure S1 in the Supporting Information), permitting the near-quantitative formation of trigonal prisms (TP), cubes (C), and pentagonal prisms (PP), with total control over position and multiplicity of the sites complementary to DNA–polymer hybrids (Table S2, Figure S3–4). The DNA–polymer conjugates (Figure 1b) consisted of a 14-mer DNA strand complementary to the cube binding regions, a pentathymidine spacer, and x hexa(ethylene) (HE, or C_{12}) units spaced by phosphodiesters. The synthesis of the conjugates is performed continuously with solid phase DNA synthesis,[4] meaning that an exact prespecified number of additions of the ethylene oligomer were added to the DNA strand, giving a high-precision polymer conjugate. HPLC purification allows separation of the target product, giving a monodisperse product in excellent yield.

The prism system permits variation of the positions and multiplicity of the binding regions that are complementary to the polymer–DNA conjugates HE_x-DNA (Figure 1c), meaning that when combined with HE_x-DNA strands anisotropic control of the polymer structure is possible in three dimensions. Manipulation of polymer chain structure in this manner has, to our knowledge, not been demonstrated by other research groups, and we anticipated that, by using a hydrophobic polymer, interesting self-assembled structures would be generated related to those we have seen using short dendritic

dx.doi.org/10.1021/ja509192n | J. Am. Chem. Soc. 2014, 136, 15767–15774

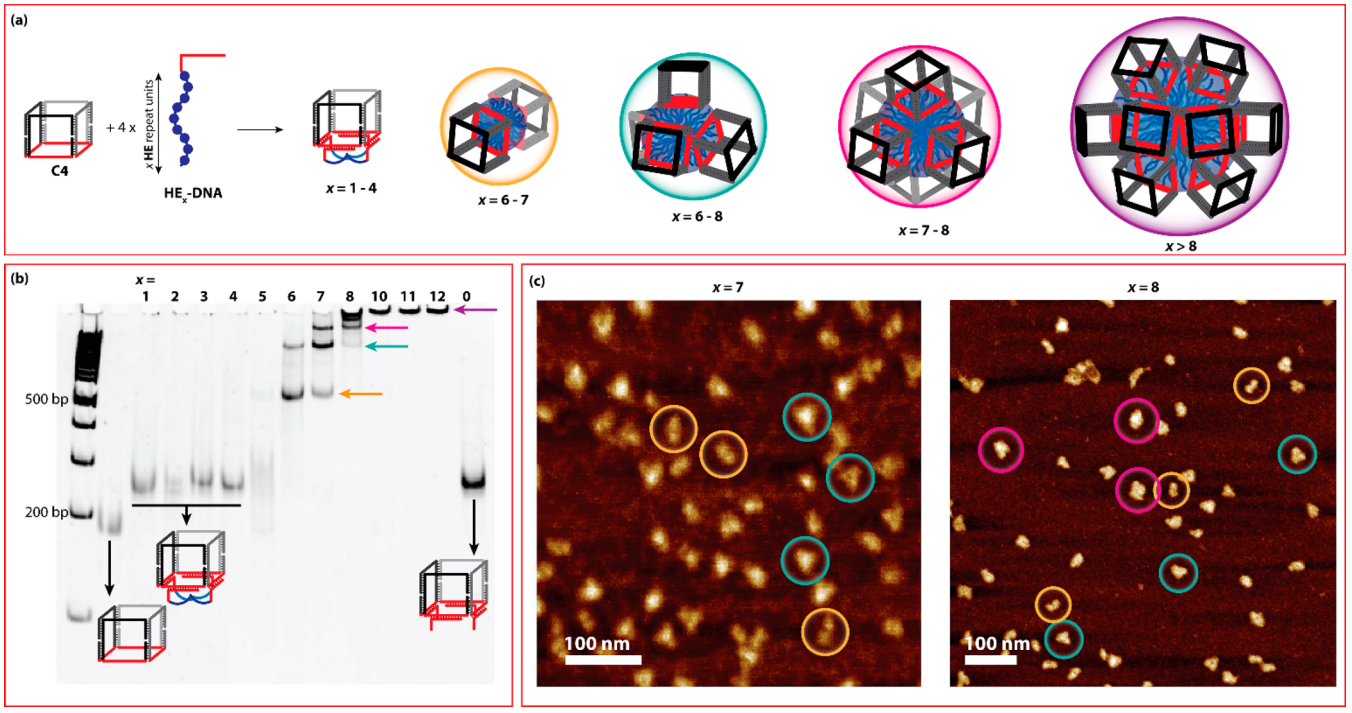

Figure 2. (a) Quantization of aggregation number observed upon stepwise increase in polymer length resulting in discrete products. (b) PAGE (5% native, TAMg buffer) analysis of product variation with polymer length, with preliminary structural assignment indicated by colored arrows. (c) AFM analysis of product distribution for x = 7 and 8, with three examples of each structure seen highlighted by colored circles. Slight change in product distribution is likely to relate to the deposition process; however, the trend toward higher assemblies with increasing polymer length is maintained.

hydrophobes.[3] Agarose gel electrophoresis (AGE) revealed that, even with a single HE_{12}-DNA attached to a cube (C1), a superstructure was formed, although the assembly was suboptimal (Figure 1c). The product purity and monodispersity improved as more HE_{12}-DNA chains were added, and the cleanest band was discerned using C4, with four binding regions on a single face. Since this geometry promotes the aggregation of proximal polymers to generate a superamphiphile, we assigned this band to a micelle of cubes (Figure 1d; see below for further characterization). The superstructures created with the other arrangements are likely to be related, although their assignment is not straightforward. When eight binding regions were present, a smeared band was observed by AGE (Figure 1c), indicating that the hydrophobic and nucleobase assembly regimes do not cooperate to give a discrete product in this arrangement.

We explored shorter HE_x-DNA strands in conjunction with C4 to establish the prerequisites for micelle formation (Figure 2a). As analyzed by poly(acrylamide) gel electrophoresis (PAGE, Figure 2b), for x = 1−4, a single band of slightly reduced mobility was seen, indicative of hybridization of the HE_x-DNA to individual cubes. The mobility of these four bands was identical, meaning that the overall size of the structure did not increase despite the longer polymers, with the implication that the polymer chains are compacted inside the cube, as seen with dendritic hydrophobes.[3] When x = 5, a smeared band was observed, whereas with x = 6−8 discrete higher order structures are seen with progressively reduced mobilities, as well as nonpenetrating material for x = 10−12. Atomic force microscopy (AFM) imaging (Figures 2c, S5−6) was used to assist in identification of the new bands. In the x = 7 system, elongated and triangular objects can be clearly seen (average height 2.2 nm), whereas with x = 8, quadrilateral structures could also be observed (average height 2.4 nm). Based upon our previous observation of hydrophobe-mediated dimerization of DNA cubes,[3] relative PAGE mobilities, and AFM images, we can unambiguously assign the first higher order band to linear dimers. Taking into consideration possible projections of 3D objects onto 2D surfaces seen by AFM, and optimal geometry for concealment of the hydrophobic segments, the next structures are likely to be tetrahedral tetramers and octahedral hexamers of cubes. By controlling the assembly conditions, we were able to tune the product distribution: larger structures can be promoted by using a higher ratio of HE_x-DNA relative to C4 (Figure S7), or working at high magnesium ion concentration, whereas the dimeric product can be selected by using low [Mg^{2+}] (Figure S8). To our knowledge, these findings constitute the first example of quantized polymer-mediated self-assembly, made possible only through the precise synthesis of DNA−polymer conjugates and their interface with 3D DNA nanostructures. The limits of this process and its potential for application are under further investigation in our laboratory.

Analysis of the C4/HE_{12} system by dynamic light scattering (DLS) gave a hydrodynamic radius (R_H) of 17.4 nm, with a polydispersity of only 8.5%, well within measurement error for a molecular species. This finding was replicable by microscopic methods, with both transmission electron microscopy (TEM) and AFM imaging spheres of a single size (Figure 3a and b). This extraordinary monodispersity has not been previously documented in similar systems, and is likely due to a combination of the purity of the polymers themselves, and the effect of having a relatively large DNA nanostructure integrated as the hydrophilic group. Depending upon the degree of compression of the DNA cubes, 15−17 cubes could be present in micelles of this size (calculations presented in Figure S9). Efforts to see the substructure by AFM were

dx.doi.org/10.1021/ja509192n | J. Am. Chem. Soc. 2014, 136, 15767−15774

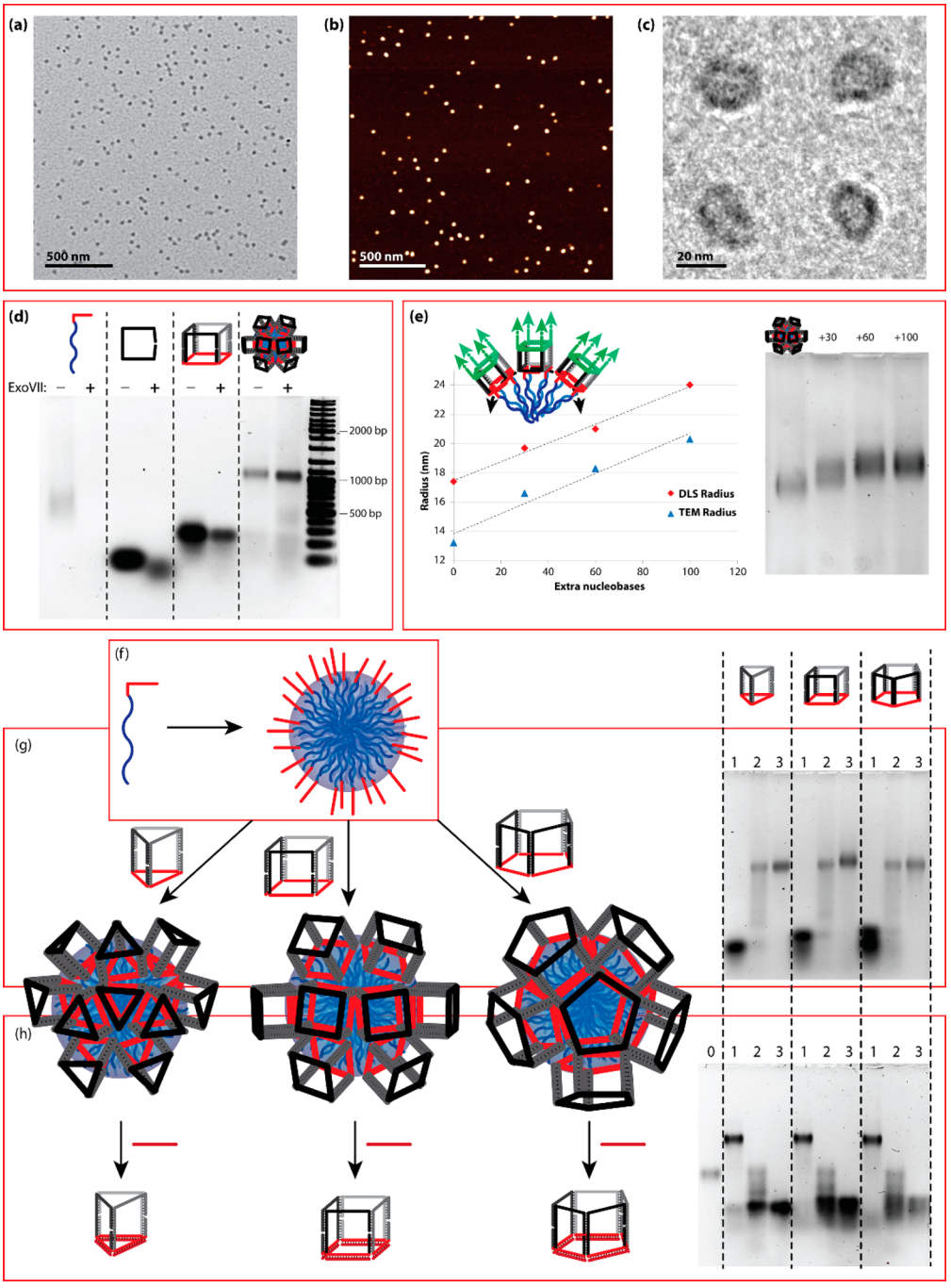

Figure 3. Characterization of C4/HE_{12} micelle. (a) TEM (R = 15.4 ± 1.2 nm). For further images see Figure S15. (b) AFM (height: 6.5 ± 1.5 nm, diameter: 44.1 ± 5.9 nm). For further images, see Figure S18. (c) Selected particles in high magnification TEM, positively stained with uranyl formate. (d) ExoVII digestion assay analyzed by native AGE (2.5%, TAMg buffer, +/− designates presence or absence of ExoVII). Native and denaturing PAGE analysis can be found in Figure S10 (molar loadings are different for the four different constructs) . (e) Increase of size through hybridization of extension strands as measured by DLS, TEM, and AGE. DLS measures the hydrodynamic radius which may include associated solvent, whereas TEM measures only the highest regions of electron density in micelle. (f–h) Appending prisms to micelles and removing them through strand displacement. (f) Preassembling HE_{12}-DNA micelle. (g) Attaching prisms by incubating preassembled micelles with preassembled prisms for 30 min at 37 °C (2.5% native AGE, TAMg buffer). For each prism: lane 1, free prism; lane 2, incubated mixture; lane 3, micelle of prisms formed by one-pot anneal (control). (h) Removing prisms from the micelle by strand displacement (2.5% native AGE, TAMg buffer). Lane 0, preassembled micelle. And for each prism: lane 1, micelle-of-prisms; lane 2, products of incubation with 20-mer complement to prism (37 °C, 30 min); lane 3, free prism control.

impeded by the overwhelming magnitude of the micelle relative to subfeatures. In uranyl acetate-stained TEM images, some variation in electron density was visible (Figure 3c), but could not be correlated with DNA structures, presumably due to deformations in the drying process. Indirect structural determination methods were therefore employed. ExoVII nuclease selectively cleaves single-stranded, open DNA over cyclic double-stranded DNA. As expected, ExoVII degraded both clip strands and HE_{12}-DNA, but neither individual cubes nor micelles-of-cubes (Figures 3d and S10), lending support to

dx.doi.org/10.1021/ja509192n | J. Am. Chem. Soc. 2014, 136, 15767−15774

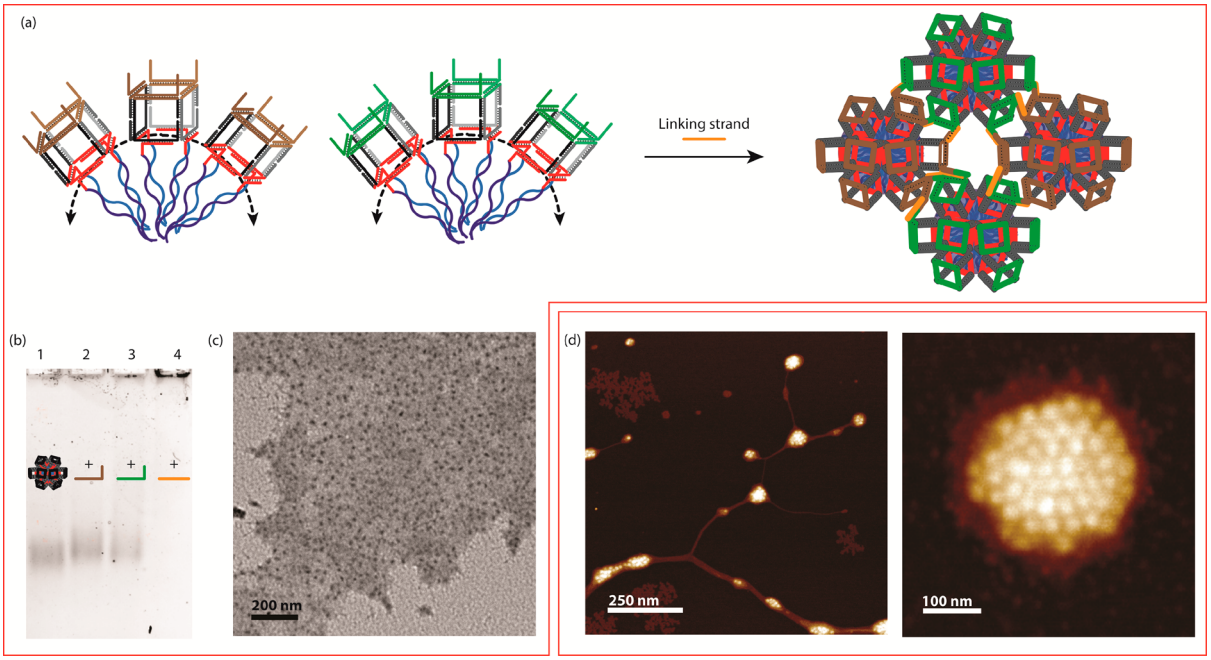

Figure 4. Assembly of micelle superstructures. (a) Cross-linking micelles through creation of two populations with pendant single stranded DNA, and their coagulation using a linking strand. (b) Analysis of the cross-linking by AGE (2.5%, TAMg buffer) shows a reduction in mobility upon addition of pendant strands, but upon cross-linking the material becomes too large to penetrate the gel. (c) TEM image of cross-linked aggregate of micelles. (d) AFM images of aggregated C4/HE_{12} micelles obtained through slow drying, and close packing of micelles within these ensembles.

the formation of intact cubes. The accessibility of the single stranded regions of the cubes (theoretically on the very exterior of the micelle) was confirmed by incubating the system with complementary strands of varying length. These strands hybridized cleanly, giving an excellent correlation between the resultant sizes as measured by TEM and DLS, AGE mobility, and the number of additional nucleobases (Figures 3e and S11−12). Thus, the cubes can hybridize to other DNA strands on their external faces without changing the spherical morphology and with predictable change in micelle size.

The integrity of the DNA nanostructure on the surface of the micelle was also assessed by preforming the HE_{12}-DNA micelles and then appending a range of prisms (TP, C, PP) of different geometry and size, using DNA hybridization. Incubating mixtures of preannealed prisms and HE_{12}-DNA micelles (Figure 3f) at 37 °C for 30 min gave the same products as when the mixtures were subjected to a one-pot long anneal (Figure 3g), suggesting that the products contained intact prisms. The same products are not obtained without preannealing, consistent with clean hybridization of the prisms within these structures. Examination of the micelles of TP and PP by DLS, AFM, and TEM (Figures S13−19) confirmed that their dimensions were very similar to those formed with cubes, regardless of sequential or one-pot anneal. Depositions for microscopy were successful at dilutions as low as 10 nM with respect to the prisms, indicating a very low critical micelle concentration. The final size of the micellar aggregate is therefore determined by the polymer chains themselves. Given that the aggregation number of HE_{12}-DNA is constant, this suggests around 20 triangular prisms TPs, or 12 pentagonal prisms PPs per micelle; that is, the number of prisms on the micelle surface varies with their geometry and size. Thus, the hybridization valency of the HE_{12}-DNA micelle can be modulated through the appendage of a prismatic DNA "adaptor."

Strand displacement reactions were used to demonstrate stimulus-specific controlled release of nanostructures, and provide absolute proof of the integrity of the prismatic nanostructures. Adding a 20-mer DNA strand complementary to the side of the prism (TP, C, or PP) to which HE_{12}-DNA was attached displaced the 14 base pair binding of HE_{12}-DNA after incubation at 37 °C for 30 min, resulting in recovery of the DNA prism and a HE_{12}-DNA micelle (Figures 3h and S20). This recovery would not be possible if the cubes were not intact, since the incubation temperature is not sufficiently high to permit the clips to rearrange. On the basis of this evidence, we can conclude that the C4/HE_{12} structures are monodisperse micelles in which the core consists of hydrophobic HE_{12} chains, and the corona is composed of intact DNA prisms which retain their addressable and potentially dynamic character, as well as their topology. We have previously shown controlled capture and release of molecular guests such as dyes or drug compounds from DNA cubes[3] and nanotubes,[20] and DNA−polymer micelles.[4] Here we have demonstrated that a multistage deployment is possible, such that large micelles can spawn their constituent DNA prisms as a response to a specific stimulus, which in turn could release their own cargo (small molecules) when directed.

As the micelles constitute a higher-order assembly of DNA nanostructures, so it was also possible to generate yet higher order assemblies of micelles, creating leads for the production of functional macroscopic materials. Superscale assembly could be achieved by appending different strands to two different populations of micelles, followed by mixing with the addition of a linking strand, creating a networked aggregate of micelles (Figure 4a). This was manifested by a nonpenetrating band in AGE (Figure 4b), and the superstructures containing micelles could be clearly seen in the 1−10 μm range using electron microscopy (Figures 4c and S21). This multicompartment material may be useful for the progressive release of therapeutic

dx.doi.org/10.1021/ja509192n | J. Am. Chem. Soc. 2014, 136, 15767−15774

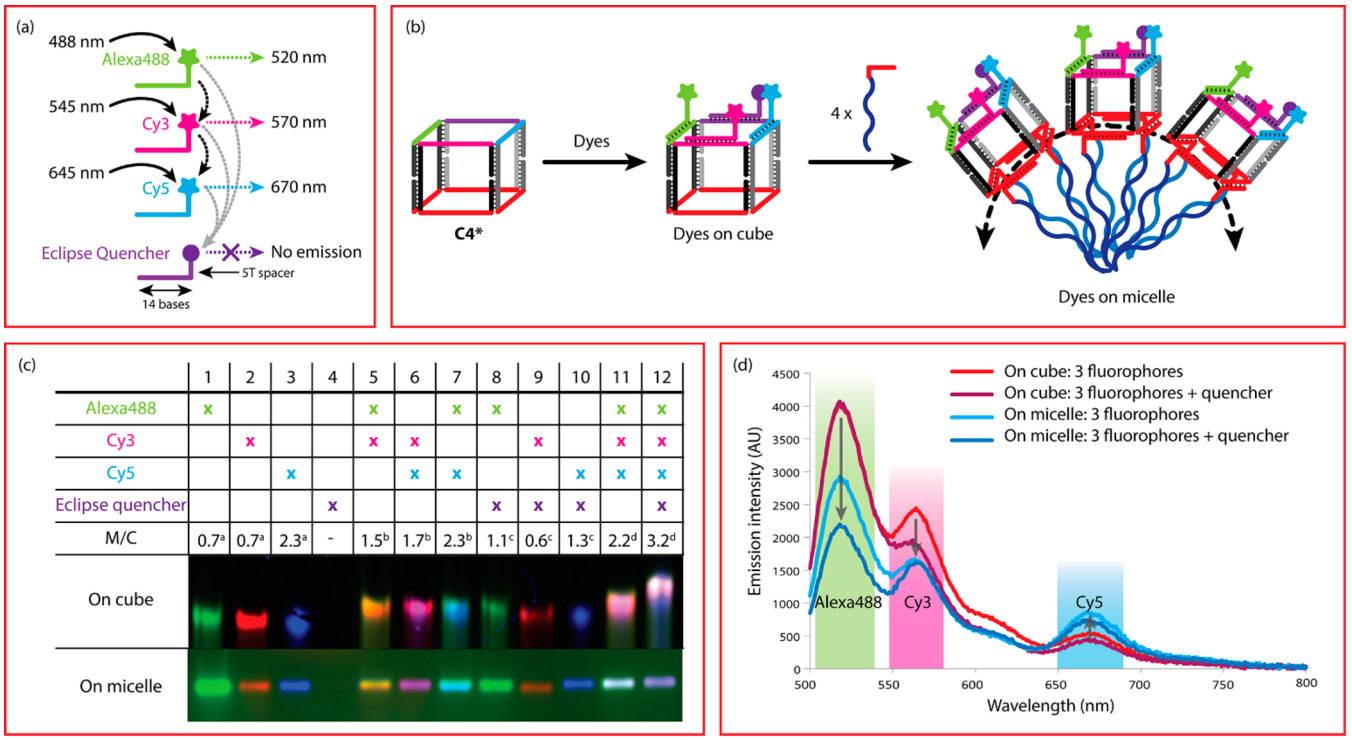

Figure 5. (a) DNA strands with conjugated dyes, showing optimal excitation wavelength (black arrows), maximum emission wavelength (colored arrows), possible energy transfer routes leading to fluorescence (dotted black arrows), and those leading to quenching (gray dotted arrows), as well as strand structure (Cy3 and Cy5 are attached at the 5′ end, whereas Alexa488 and EQ are at the 3′ terminus). (b) Programmed arrangement of dye strands on an appropriately designed DNA cube, and subsequent formation of a micelle. (c) Overlayed multichannel fluorescence scans of gel electrophoretogram bands arising from dyes on cube (5% PAGE) and the micelle of cubes (2.5% AGE). Each dye was excited at its own wavelength, and the expected emission of that dye was collected in the appropriate range (the first three lanes show minimal overlap). Alexa488 = green, Cy3 = red, Cy5 = blue. Also given in the table are comparisons between the micelle and the cube fluorescence, taken from fluorescence spectroscopy. Superscripts designate: [a]single dye fluorescence intensity; [b]relative 2-dye FRET efficiency; [c]relative quenching efficiency; [d]relative three-dye FRET efficiency. (d) Fluorescence spectra (exciting at 488 nm) showing increase in energy transfer from Alexa488 to Cy5 via Cy3 when cubes are assembled into micelles.

small molecules or nucleic acids using different stimuli. Multimicellar aggregates could also be obtained using non-specific interactions. Slow drying of a solution of micelles onto mica for AFM characterization resulted in collection of micelles into hexagonally packed groups (Figures 4d and S22). This result suggests that crystallization, akin to that seen for spherical nucleic acids,[21] may be possible with this system.

The addressable nature of the system was further confirmed by arranging dyes on its surface, creating a light harvesting cascade. Natural photosynthetic systems use light in the most efficient way through the optimal arrangement of energy channelling chromophores. Hence, significant efforts have been directing at organizing dyes on the nanoscale,[22−26] including use of DNA nanostructures[27−30] since proximal arrangement of dyes permits through-space energy transfer via the Förster resonance energy transfer (FRET) mechanism. The fluorescent dye pairs Alexa488/Cy3 and Cy3/Cy5 have good overlap between the emission of the shorter wavelength dye and the excitation of the longer wavelength dye and are thus good FRET partners, whereas Alexa488 and Cy5 have poor overlap. The absorbance of Eclipse Quencher (EQ) coincides with all the fluorophores, but is greatest with Cy3 (Figure 5a). The cube system was modified such that four distinct sequences were displayed on each edge of its exterior face (C4*, Figure 5b), and complementary strands terminated with Alexa488, Cy3, Cy5, and EQ dyes were synthesized. The dimensions of the cube and the structure of the dye strands mean that the distances between the dyes are suboptimal for FRET (average distance ca. 8 nm). Additionally, conformational freedom means that at any one time the distance between donor and acceptor may be beyond the FRET distance. When the cubes are gathered together in a micelle, it is expected that FRET will be enhanced by bringing multiple copies of dyes into a single structure, making the presence of an acceptor dye near a donor much more likely. The fluorescence properties of dyes appended individually or in groups to free cubes or micelle-bound cubes were first probed qualitatively using multichannel imaging of gels (Figure 5c). These results confirmed that the dyes had hybridized correctly to both the free and micelle-bound cubes. Pairwise Alexa488 → Cy3 (Figure 4c, lane 5), Cy3→ Cy5 (lane 6), and even Alexa488 → Cy5 (lane 7) FRET was observed (Figures S23 and 24), and each of the dyes was partially quenched by EQ (lanes 8−10). Inclusion of all three fluorophores produced a light-harvesting Alexa488 → Cy3 → Cy5 FRET cascade (lane 11 and Figure 4d, red trace), which could be further quenched in a four-dye system (lane 12 and Figure 5d, purple trace).

Quantitative assessment comparison between the free and micelle-bound cube systems was obtained using a scanning fluorimeter (Figures 5c (M/C), d and S25−28). Using the free cube, individual fluorescence of single dyes was observed as expected. In the two dye systems, significant emission was seen from the longer wavelength dye upon exciting the higher frequency dye, and the intensity of all the dyes was reduced

dx.doi.org/10.1021/ja509192n | J. Am. Chem. Soc. 2014, 136, 15767−15774

when combined with EQ, Cy3 being the most affected. When all three fluorescent species were present, the emission of Cy5 relative to Alexa488 (λ_{ex} = 488 nm) was increased by a factor of 1.7. The same trend occurred with the micellar system, although the differences were made starker. In the single-dye systems, there was a 30% reduction of fluorescence of Alexa488 and Cy3 relative to the cube, attributed to aggregation-induced self-quenching, while the Cy5 emission in the micelle was 2.3 times its free-cube value. Two-dye FRET was enhanced by factors of 1.5 to 2.3 upon micellization, while quenching efficiency was enhanced marginally for Alexa488 and Cy5. Quenching was reduced for Cy3, probably an artifact arising from Cy3 being already partly self-quenched in the micelle. Again, the inclusion of Cy3 as a bridge dye between Alexa488 and Cy5 increased the Cy5 emission, with the effect being 2.3 times larger in the micelle. The effect of completing the dye quartet by addition of EQ was also affected by aggregation: in the micelle the quencher acted almost exclusively on Alexa488 instead of Cy3 in the free cube. Although the output was quenched slightly, in the 4-dye system, the Cy5/Alexa488 emission ratio was now 3.2 times greater in the micelle than the cube. We have thus shown that by using polymer self-assembly to create a superstructure of DNA nanostructures, combinations of fluorophores can be produced in a programmed fashion, and that interactions between the dyes can be modified to generate enhanced light harvesting cascades. We have intentionally designed a suboptimal system to highlight the effect of micellization; much greater enhancements should be expected from more precisely designed systems.

CONCLUSIONS AND OUTLOOK

We have demonstrated that precision-synthesized polymers can be used orthogonally in conjunction with DNA nanotechnology to create higher order structures with an unprecedented level of control over the aggregation number, including the first example of quantized polymer self-assembly. By using an orthogonal assembly system, we are able to access a library of larger, functional DNA nanostructures without the need for a large number of different strands or a high level of sequence complexity; indeed, only four to six strands were used for the micelles-of-prisms. No additional polymers or surfactants were required. We have shown that the DNA nanostructures are intact on the surface of the micelles, that they retain in every way their addressable character, and that it is the polymer aggregation number which determines how many nanostructures are appended.

We have presented controlled release of daughtership nanostructures using specific stimuli, which is especially relevant for drug delivery; the nanoscale properties of the carriers can be changed dramatically through release. In particular, the size of the micelles is appropriate for targeted cancer combat strategies through the enhanced permeation and retention effect.[31] The strand-displacement methods we have used in this proof-of-principle could be replaced with biologically relevant aptamer or antisense interactions, and the exterior could be modified to optimize nuclease stability, cell permeation, or other biological recognition events through self-assembled multivalency. The versatility of the micelle as a scaffold has been shown in the creation of a four-dye light harvesting array.

The modularity of the system means that its applicability is extremely broad: alteration of the polymer, the DNA nanostructure, or the appended species is straightforward. This is the first exploration into the parameter space open to the interface of precision polymers and DNA nanostructures, and we anticipate that many more exciting results can arise from this method.

ASSOCIATED CONTENT

Supporting Information

Figures S1−S28, Tables S1−S3, detailed experimental procedures, and further data. This material is available free of charge via the Internet at http://pubs.acs.org.

AUTHOR INFORMATION

Corresponding Author

hanadi.sleiman@mcgill.ca

Notes

The authors declare no competing financial interest.

ACKNOWLEDGMENTS

The authors acknowledge the Natural Sciences and Engineering Research Council of Canada (NSERC), the Canada Foundation for Innovation (CFI), the Centre for Self-Assembled Chemical Structures (CSACS), and the Canadian Institute for Advanced Research (CIFAR) for financial support. C.J.S. thanks NSERC for a Banting Postdoctoral Fellowship. T.G.W.E. thanks Canadian Institutes of Health Research (CIHR) for a Drug Development Training Program (DDTP) scholarship. H.F.S. is a Cottrell Scholar of the Research Corporation. We thank Graham Hamblin for assistance with the figures.

REFERENCES

(1) Seeman, N. C. *Mol. Biotechnol.* **2007**, *37*, 246−257.
(2) Mai, Y.; Eisenberg, A. *Chem. Soc. Rev.* **2012**, *41*, 5969−5985.
(3) Edwardson, T. G. W.; Carneiro, K. M. M.; McLaughlin, C. K.; Serpell, C. J.; Sleiman, H. F. *Nature Chem.* **2013**, *5*, 868−875.
(4) Edwardson, T. G. W.; Carneiro, K. M. M.; Serpell, C. J.; Sleiman, H. F. *Angew. Chem., Int. Ed.* **2014**, *53*, 4567−4571.
(5) Jeong, J. H.; Park, T. G. *Bioconjugate Chem.* **2001**, *12*, 917−923.
(6) Talom, R. M.; Fuks, G.; Kaps, L.; Oberdisse, J.; Cerclier, C.; Gaillard, C.; Mingotaud, C.; Gauffre, F. *Chem.—Eur. J.* **2011**, *17*, 13495−13501.
(7) Kwak, M.; Herrmann, A. *Angew. Chem., Int. Ed.* **2010**, *49*, 8574−8587.
(8) Chien, M.-P.; Rush, A. M.; Thompson, M. P.; Gianneschi, N. C. *Angew. Chem., Int. Ed.* **2010**, *49*, 5076−5080.
(9) Li, Z.; Zhang, Y.; Fullhart, P.; Mirkin, C. A. *Nano Lett.* **2004**, *4*, 1055−1058.
(10) Teixeira, F., Jr.; Rigler, P.; Vebert-Nardin, C. *Chem. Commun.* **2007**, 1130−1132.
(11) Caseli, L.; Pascholati, C. P.; Teixeira, F., Jr.; Nosov, S.; Vebert, C.; Müeller, A. H. E.; Oliveira, O. N., Jr. *J. Colloid Interface Sci.* **2010**, *347*, 56−61.
(12) Carneiro, K. M. M.; Hamblin, G. D.; Hanni, K. D.; Fakhoury, J.; Nayak, M. K.; Rizis, G.; McLaughlin, C. K.; Bazzi, H. S.; Sleiman, H. F. *Chem. Sci.* **2012**, *3*, 1980−1986.
(13) Wilks, T. R.; Bath, J.; de Vries, J. W.; Raymond, J. E.; Herrmann, A.; Turberfield, A. J.; O'Reilly, R. K. *ACS Nano* **2013**, *7*, 8561−8572.
(14) Langecker, M.; Arnaut, V.; Martin, T. G.; List, J.; Renner, S.; Mayer, M.; Dietz, H.; Simmel, F. C. *Science* **2012**, *338*, 932−936.
(15) Wang, R.; Wang, C.; Cao, Y.; Zhu, Z.; Yang, C.; Chen, J.; Qing, F.-L.; Tan, W. *Chem. Sci.* **2014**, *5*, 4076−4081.
(16) Zhou, C.; Wang, D.; Dong, Y.; Xin, L.; Sun, Y.; Yang, Z.; Liu, D. *Small* **2014**, DOI: 10.1002/smll.201401576.
(17) List, J.; Weber, M.; Simmel, F. C. *Angew. Chem., Int. Ed.* **2014**, *53*, 4236−4239.

(18) McLaughlin, C. K.; Hamblin, G. D.; Hänni, K. D.; Conway, J. W.; Nayak, M. K.; Carneiro, K. M. M.; Bazzi, H. S.; Sleiman, H. F. *J. Am. Chem. Soc.* **2012**, *134*, 4280−4286.
(19) Conway, J. W.; McLaughlin, C. K.; Castor, K. J.; Sleiman, H. *Chem. Commun.* **2013**, *49*, 1172−1174.
(20) Lo, P. K.; Karam, P.; Aldaye, F. A.; McLaughlin, C. K.; Hamblin, G. D.; Cosa, G.; Sleiman, H. F. *Nature Chem.* **2010**, *2*, 319−328.
(21) Cutler, J. I.; Auyeung, E.; Mirkin, C. A. *J. Am. Chem. Soc.* **2012**, *134*, 1376−1391.
(22) Xue, B.; Li, Y.; Yang, F.; Zhang, C.; Qin, M.; Cao, Y.; Wang, W. *Nanoscale* **2014**, *6*, 7832−7837.
(23) Webber, S. E. *Chem. Rev.* **1990**, *90*, 1469−1482.
(24) Thompson, B. C.; Fréchet, J. M. J. *Angew. Chem., Int. Ed.* **2008**, *47*, 58−77.
(25) Gust, D.; Moore, T. A.; Moore, A. L. *Acc. Chem. Res.* **1993**, *26*, 198−205.
(26) Zou, Q.; Zhang, L.; Yan, X.; Wang, A.; Ma, G.; Li, J.; Möhwald, H.; Mann, S. *Angew. Chem., Int. Ed.* **2014**, *53*, 2366−2370.
(27) Garo, F.; Häner, R. *Angew. Chem., Int. Ed.* **2012**, *51*, 916−919.
(28) Woller, J. G.; Hannestad, J. K.; Albinsson, B. *J. Am. Chem. Soc.* **2013**, *135*, 2759−2768.
(29) Dutta, P. K.; Varghese, R.; Nangreave, J.; Lin, S.; Yan, H.; Liu, Y. *J. Am. Chem. Soc.* **2011**, *133*, 11985−11993.
(30) Holzhauser, C.; Rubner, M. M.; Wagenknecht, H.-A. *Photochem. Photobiol. Sci.* **2013**, *12*, 722−724.
(31) Maeda, H.; Wu, J.; Sawa, T.; Matsumura, Y.; Hori, K. *J. Controlled Release* **2000**, *65*, 271−284.